



# ENHANCING ACCURACY IN EMCCD MEASUREMENTS OF LUMINESCENCE FROM SINGLE GRAINS THROUGH MINIMISING SIGNAL CROSSTALK

GRZEGORZ ADAMIEC<sup>1</sup>, GEOFF A.T. DULLER<sup>2</sup> and MATT GUNN<sup>3</sup>

<sup>1</sup>*Division of Geochronology and Environmental Isotopes, Institute of Physics – Centre for Science and Education, Silesian University of Technology, ul. S. Konarskiego 22B, 44-100, Gliwice, Poland*

<sup>2</sup>*Department of Geography and Earth Sciences, Aberystwyth University, Ceredigion, SY23 3DB, United Kingdom*

<sup>3</sup>*Department of Physics, Aberystwyth University, Ceredigion, SY23 3BZ, United Kingdom*

Received 10 February 2025

Accepted 28 May 2025

## Abstract

This study addresses the challenge of signal crosstalk in luminescence measurements from single sand-sized mineral grains, utilising Electron-Multiplying Charge-Coupled Devices (EMCCD) for imaging. Crosstalk, or signal interference between adjacent grains, may significantly hamper the accuracy of luminescence analysis of signals emitted by single mineral grains. The research aims to minimise crosstalk, thereby enhancing the integrity of the luminescence data from each grain.

The effects of altering the aperture size and the spacing between grains on the sample disc are investigated using the 110°C thermoluminescence (TL) peak of quartz as an example. Specifically, the introduction of a newly designed sample disc with increased spacing between grain holes shows promising results in mitigating signal overlap, as evidenced by the experimental data. In particular, we demonstrate that the new design dramatically decreases signal crosstalk, enabling reliable automatic data analysis with minimal interference.

The study offers practical solutions for enhancing the reliability of single-grain based luminescence chronologies and dosimetric assessments. By minimising signal crosstalk, more precise and reliable analyses of thermoluminescence and OSL signals can be obtained.

To demonstrate the potential of the new design, for the first time, we show the estimation of trap parameters of the 110°C peak in quartz at a single-grain level using an EMCCD camera, comparing it with the lifetime of the electrons in the 110°C trap measured directly through storage experiments.

## Keywords

Luminescence, Crosstalk, EMCCD, Single Grains, Quartz, Dosimetry, Geochronology

## 1. Introduction

Stimulated luminescence is widely used for measurements of the ionising radiation dose received by samples. It finds application in medical, personal and accident dosimetry (e.g. Yukihiro *et al.*, 2014) and is widely used for dating geological and archaeological samples (Roberts *et al.*, 2015). Recent advances in luminescence studies of mineral grains have resulted in novel methodologies that

significantly enhance our understanding of the variability inherent in these materials. Traditionally, researchers have relied on multiple-grain aliquots or single-grain focussed laser systems to measure luminescence, with each method presenting its own set of limitations. Multiple-grain aliquots offer simplicity but obscure individual grain behaviour, leading to a scatter in the signal (e.g. Wallinga, 2002). Focussed laser systems (Duller *et al.*, 1999, Bailiff and Mikhailik, 2003, Bøtter-Jensen *et al.*, 2003), while providing resolution at the grain level, are only able to look at optically stimulated signals and are unable to measure thermoluminescence (TL) emitted by individual grains,

Corresponding author: G. Adamiec  
e-mail: [grzegorz.adamiec@polsl.pl](mailto:grzegorz.adamiec@polsl.pl)

meaning that hand-picking of individual grains is the only solution for TL measurements (e.g. Adamiec, 2000).

Imaging of luminescence from natural minerals using image intensifiers (Templer and Walton, 1985), imaging photon detectors (Smith *et al.*, 1991), and charge-coupled devices (Duller *et al.*, 1997) has been attempted previously, but the introduction of thermoelectrically-cooled electron-multiplying charge-coupled devices (EMCCD) represents a significant step forward. These devices offer the potential to capture spatially resolved measurements of luminescence with low read noise and high quantum efficiency across a wavelength range of typically 300 to 1000 nm. This allows for comprehensive dosimetry studies and in-depth investigations into the physics of luminescent materials, with applications ranging from geochronology to accident dosimetry. Notably, the use of EMCCD facilitates the analysis of TL glow curves and OSL properties across large numbers of grains under consistent temperature conditions – addressing a longstanding challenge in luminescence studies.

Whether using focussed laser systems or imaging systems, the rationale for using such systems is to be able to measure the luminescence signal from a single mineral grain without contribution from other grains on the sample. Unfortunately, contributions from nearby grains occur in both types of systems, and this unwanted signal is termed crosstalk. For focussed laser systems, where optically stimulated luminescence is measured, the crosstalk (stimulation crosstalk) arises from stray light from the laser beam (Duller, 2012) striking grains other than the measured one. Since the laser power on these other grains will be much lower than the power on the grain being measured, this tends to generate what appears to be a slow component (Singarayer and Bailey, 2003) in the quartz OSL signal, and using such focussed laser systems is likely to lead to overestimates of the frequency of grains with a slow component and to overestimate the magnitude of this slow component (e.g. Fig 3b, Bulur *et al.*, 2002).

Imaging systems are not affected by crosstalk arising from optical stimulation but do suffer from crosstalk for other reasons. Crosstalk for imaging systems arises for two primary reasons, firstly because of various types of aberration (spherical aberration, chromatic aberration, coma, astigmatism etc) in the optics used to focus the luminescence emitted from the sample onto the detector, and secondly because the light being observed arises from within the sample and is emitted uniformly in all directions and this may reflect off other grains or parts of the sample holder or chamber. Where individual mineral grains are to be analysed, the severity of the crosstalk due to scattering of the light will be highest if a flat sample holder is used (e.g. Gribenski *et al.*, 2015), and can be reduced by placing each grain in a recess drilled into the sample holder as designed by Duller *et al.* (1999). These sample holders are called single grain discs and are designed with an array of holes of a diameter and depth such that one mineral grain can fit within each hole. Such discs have two main

advantages. Firstly, they reduce the lateral scattering of light. Secondly, they physically separate the grains and hold them in a known geometry (typically 600  $\mu\text{m}$  between grain centres), avoiding the need to attempt to define grain locations and boundaries by image analysis (cf. Greulich *et al.*, 2015; Mittelstraß and Kreutzer, 2021), making data reduction much simpler (e.g. Kook *et al.*, 2015).

Kook *et al.* (2015) developed an imaging EMCCD system for the Risø TL/OSL instrument. The TL and OSL signals from natural minerals that the system is designed to look at are often weak, and Kook *et al.* (2015) recognised the conflicting design aims of maximising numerical aperture to increase light collection or reducing numerical aperture to deliver a well-focussed image and reduce crosstalk. Using a single grain disc with 300  $\mu\text{m}$  diameter holes drilled with their centres spaced 600  $\mu\text{m}$  apart, and using a region of interest 450  $\mu\text{m}$  in diameter, they demonstrated that crosstalk between grain positions was about 0.8%. That is to say that if a grain in one hole on the single grain disc emitted 100,000 photons, 800 photons from that grain would be observed in the part of the image where an adjacent grain would sit. Since 2015, the instrument has been modified with the addition of a computer-controlled iris in the optical path, providing the potential for improving image quality by reducing the aperture. This new instrument has been used in several studies (e.g. Durcan and Duller 2022, 2024), but little characterisation of its performance has been undertaken. De Boer *et al.* (2024) have measured crosstalk for this new version of the instrument, and using the same sized region of interest as Kook *et al.* (2015), they get a value of 5.5%, but the reason for this being almost six times larger than previously measured is not clear. Rather surprisingly, De Boer *et al.* (2024) found that there was no systematic change in signal crosstalk or in signal intensity as the aperture was changed. From first principles, one would expect that reducing the aperture would improve image resolution and thus lower crosstalk, but at the cost of signal intensity, and it is not clear why this was not seen in that study.

As we continue to use and refine imaging techniques, it is crucial to ensure that the luminescence signal detected is indeed from the targeted grain, uncompromised by adjacent grains' stray light. This problem is particularly important because the brightness of quartz grains originating from a single sample may span a few orders of magnitude (e.g. Duller, 2008). Analysis of single grains of quartz from geological or archaeological sites has repeatedly shown that only a small proportion of grains emit a detectable signal (e.g. Duller *et al.*, 2000), meaning that it would be expected for only a few grains (~2 to 10 grains) on a single grain disc to have any measurable signal. The ongoing optimisation is key to the integrity of single-grain analysis and underpins the confidence in our data as we unravel the complexities of luminescent minerals.

In the current paper, we investigate the influence of aperture on crosstalk and signal intensity for the Risø EMCCD unit. The main motivation for undertaking this

research was to enable the full exploitation of the capabilities of EMCCD cameras in luminescence investigations. We explore changing the spacing between grain holes on a single-grain disc and discuss the results we obtained. Subsequently, we discuss the possibility of automated detection of a crosstalk signal. We propose a new design of discs for single grain measurements using EMCCD, and we show an example of their application in determining the kinetic parameters of the “110°C” TL peak in individual quartz grains.

## 2. Instrumental setup and analysis

### 2.1 Instrument

In the present study, we have employed a setup featuring an Evolve™ electron-multiplying charge-coupled device (EMCCD) cooled to -80°C, as detailed by Kook *et al.* (2015). This EMCCD, with its 512 by 512-pixel array, is mounted onto a Risø TL/OSL DA-20 reader, replacing the conventional photomultiplier tube, thus enhancing our capability to detect emissions effectively from quartz. The peak quantum efficiency of the EMCCD (~90%) is between 400 and 700 nm, but even at 340 nm, the wavelength used for the detection of luminescence from quartz in our experiments, the quantum efficiency (~35%) is larger than that for a bialkali photomultiplier tube (Kook *et al.*, 2015) which is most frequently used for this purpose. The EMCCD is operated in EM-gain mode when measuring luminescence signals, but not when collecting visible images for registration purposes.

The system's optics, comprising a lens setup with a magnification of 0.8, focus the emissions onto the CCD chip's surface. Each detector pixel measures 16 µm by 16 µm, resulting in an effective pixel size at the sample plane of *ca.* 20 µm by 20 µm after magnification. This setup allows for a maximum imaging area of 10.24 mm by 10.24 mm on the sample. The instrument is able to adjust the focus under computer control, compensating for the small variations in the focal plane that occur as a function of wavelength. The DASH EMCCD unit used in the experiments reported here is different to that reported by Kook *et al.* (2015), as an upgrade by the manufacturer has added a motorised iris under computer control, which enables the selection of apertures ranging from 21.9 mm to 2.2 mm. Hoya U-340 and Schott UG-11 glass filters, with a combined thickness of 4 mm, have been used. This filter combination transmits light at 340 nm with an FWHM of 85 nm and filters out the blackbody radiation at elevated temperatures. In section 4, the filter Schott BG-39 was used, the rationale being given there.

### 2.2 Sample

In our study, we used the sample Aber105/KB15 (grain size 180–250 µm; Duller *et al.*, 2015) from Kalambo Falls, Zambia, known for its bright OSL. The sample was prepared as loose grains of quartz, typically 180 to 250 µm in diameter, using a combination of physical and chemical

methods to separate quartz from the other minerals present. Duller *et al.* (1999) designed an aluminium disc to fit within the automated Risø TL/OSL reader, which could hold grains in defined positions, physically separated from each other. This single-grain aluminium disc is 9.8 mm in diameter and has an array of 300 µm diameter holes drilled 300 µm deep into the surface of the disc. Three holes 500 µm in diameter are drilled through the disc near its periphery. These three holes do not contain the sample but are used solely for assessing the position of the disc relative to the imaging system. The current configuration of these sample discs has an array of 10 by 10 holes, with a spacing of 600 µm between hole centres (see e.g. Kook *et al.*, 2015).

### 2.3 Sample disc manufacture

A second type of sample holder was used later in this research, designed to reduce the impact of crosstalk. The disc had the same external diameter (9.8 mm) and the same three locating holes as that described above, but instead of an array of 10 by 10 holes, this new disc has an array of 7 by 7 holes, allowing the spacing between hole centres to be increased from 600 µm to 850 µm. The hole diameter was kept at 300 µm. These new discs were fabricated from stainless steel and cut using a laser engraving system. The rationale for this design modification is explained in section 3, along with data illustrating the advantages of this design.

### 2.4 Data processing

A suite of custom Python functions and classes was developed to facilitate the comprehensive analysis of luminescence signals from disc samples. This software is designed to automatically detect positioning markers on the discs, which are critical for accurate positioning of regions of interest. Utilising image processing libraries such as OpenCV (Bradski, 2000) and scikit-image (van der Walt *et al.*, 2014), the software identifies these markers through edge detection and Hough Circle Transform algorithms, ensuring precise location even in varied lighting.

The core functionality extends beyond marker detection, offering tools for signal integration over specified circular regions of interest (ROIs). Furthermore, the software supports the generation of transects of a defined width, enabling the examination of the luminescence signal between any two points on the disc. This capability is invaluable for studying spatial variations in signal intensity. By automating critical tasks, the software enables rapid analysis of large numbers of grains, making it a very useful tool for single-grain luminescence research.

All glow curves were smoothed using the Savitzky-Golay filter (Savitzky and Golay, 1964) implemented in SciPy.signal package (Virtanen *et al.*, 2020) with a window length of 15 channels and a 3<sup>rd</sup> degree polynomial. Prior to analysis, the background signal was subtracted. In the experiments described in section 3, where only four grains were placed on the sample disc, background measurements were taken from grain positions or transects

located far from the holes containing grains. It was confirmed that the subtracted signal showed no visible TL peaks.

In the experiments where all holes were filled with grains (section 3, Fig. 8 and section 4), the background was obtained from a subsequent heating of the same sample grain positions under identical thermal conditions but without prior dosing.

### 3. Spatial distribution of luminescence arising from a single grain

To optimise the acquisition of spatially resolved luminescence, we first decided to explore in detail the spatial pattern of luminescence emitted from single grains mounted on our sample holder. To do this, an experiment was undertaken in which four grains of quartz were placed by hand under white light in a single-grain disc with an array of 10 by 10 holes (300  $\mu\text{m}$  diameter) in positions (3, 3), (3, 8), (8, 3) and (8, 8) corresponding to numbers 23, 28, 73, and 78 (Fig. 1, bottom right). The positions are defined as in the Risø Sequence Editor software, where grain (1, 1) occupies the top right position of the 10 by 10 grid. We explored the influence of the aperture on the image quality, the intensity of the luminescence signal, and the spatial extent of the signal in relation to the position of the grain.

#### 3.1 Aperture

A series of measurements was undertaken using apertures varying from 21.9 mm to 2.2 mm (the full range of the iris). For each measurement cycle, the disc received a dose of 280 Gy, and immediately following this irradiation, the disc was heated at  $1^\circ\text{C s}^{-1}$  to a temperature of  $220^\circ\text{C}$ . The TL signal emitted during the heating was recorded, with one frame collected with the EMCCD in EM-gain mode every two seconds (equivalent to an increase of  $2^\circ\text{C}$ ).

A region of interest 300  $\mu\text{m}$  in diameter was used to sum the signal from grain position 23, the brightest of the four grains. A typical TL glow curve is shown in Fig. 2a. The sequence of irradiation and TL measurement was repeated while varying the aperture from 21.9 mm to 2.2 mm, and the impact upon the signal intensity is shown in Fig. 2b. For this data, the intensity is fitted by the power function

$$\text{TL} = 560.8 \cdot \text{Aperture}^{1.7} \quad (3.1)$$

where the TL indicates counts integrated over the temperature range  $50\text{--}100^\circ\text{C}$  and the aperture is given in mm, confirming the strong dependence of the signal on the aperture. There is a trade-off to be found between the resolution of the image and the size of the aperture. We conclude that unless we are dealing with exceptionally bright luminescence signals, using small apertures is a seriously limiting factor, and for that reason, a large aperture should be used.

#### 3.2 Signal crosstalk

The data collected for Fig. 2 can also be displayed as images, showing the spatial distribution of luminescence observed from the four grains. For measurements using different apertures, Fig. 1 shows the result of summing all the images collected up to the maximum temperature of  $220^\circ\text{C}$ . For the smallest aperture ( $A_p=2.2$  mm), the TL emission is spatially well resolved, and the size of the TL feature appears to match the size of the grains used. As the aperture used during data collection is increased, the TL appears to originate from a wider area, presumably resulting from increasing aberration. This suggests that increased crosstalk will also be seen as the aperture is increased.

To explore the spatial pattern of luminescence in the current configuration, the luminescence images collected by the EMCCD for apertures of 21.9 and 10 mm were processed to extract a transect *ca.* 6 mm in length, 100  $\mu\text{m}$  in width, across positions 21 to 30 on the single grain disc (Fig. 3a). Positions 23 and 28 along this transect contain grains (as seen in Fig. 2), and these grains' emissions are clearly visible in Figs. 3b (aperture 21.9 mm) and 3c (aperture 10 mm). Routine analysis (Kook *et al.*, 2015) of the emission from positions 21 to 30 would define regions of interest (ROI) centred on each grain (these ROIs with a diameter of 300  $\mu\text{m}$  are visible in Fig. 3a as green circles as well as shaded stripes in Fig. 3b and 3c; they coincide with the grain holding holes). The pattern of the logarithm of the emission along the transect clearly shows that the signal significantly spills over to the adjacent positions for both apertures, the spillover being significantly reduced for the aperture of 10 mm (Fig. 3c). However, the signal in this case is reduced nearly fourfold according to Eq 3.1 ( $\frac{560.8 \cdot 21.9^{1.7}}{560.8 \cdot 10^{1.7}} = 3.8$ ).

To illustrate the potential for misinterpreting this data set, TL glow curves obtained for grain 23 and the surrounding positions for the aperture of 21.9 mm are shown in Fig. 4. While position 23 has the most intense signal (more than 7000 counts at  $73^\circ\text{C}$ ), TL peaks are also seen for the surrounding positions. Had we not known these positions were empty, these would have been interpreted as TL glow curves originating from different grains but with similar properties. These plots clearly show how easy it might be to incorrectly interpret signals originating from single grains.

Further, Fig. 5 shows the crosstalk between position 23 and the adjacent positions. The crosstalk is calculated from the formula:

$$\eta_{\%} = \frac{s_n - s_{23}}{s_{23}} \cdot 100\% \quad (3.2)$$

where  $s_n$  is the signal from the  $n$ -th position and  $s_{23}$  is the signal from position 23. Using the original optics design for this EMCCD system (but without a variable iris), Kook *et al.* (2015) assessed crosstalk to be 0.8%. De Boer *et al.* (2024) used a system with a variable iris and obtained a value for crosstalk of 5.5%. Our data are similar to the value of Kook *et al.* (2015) but reveal some additional

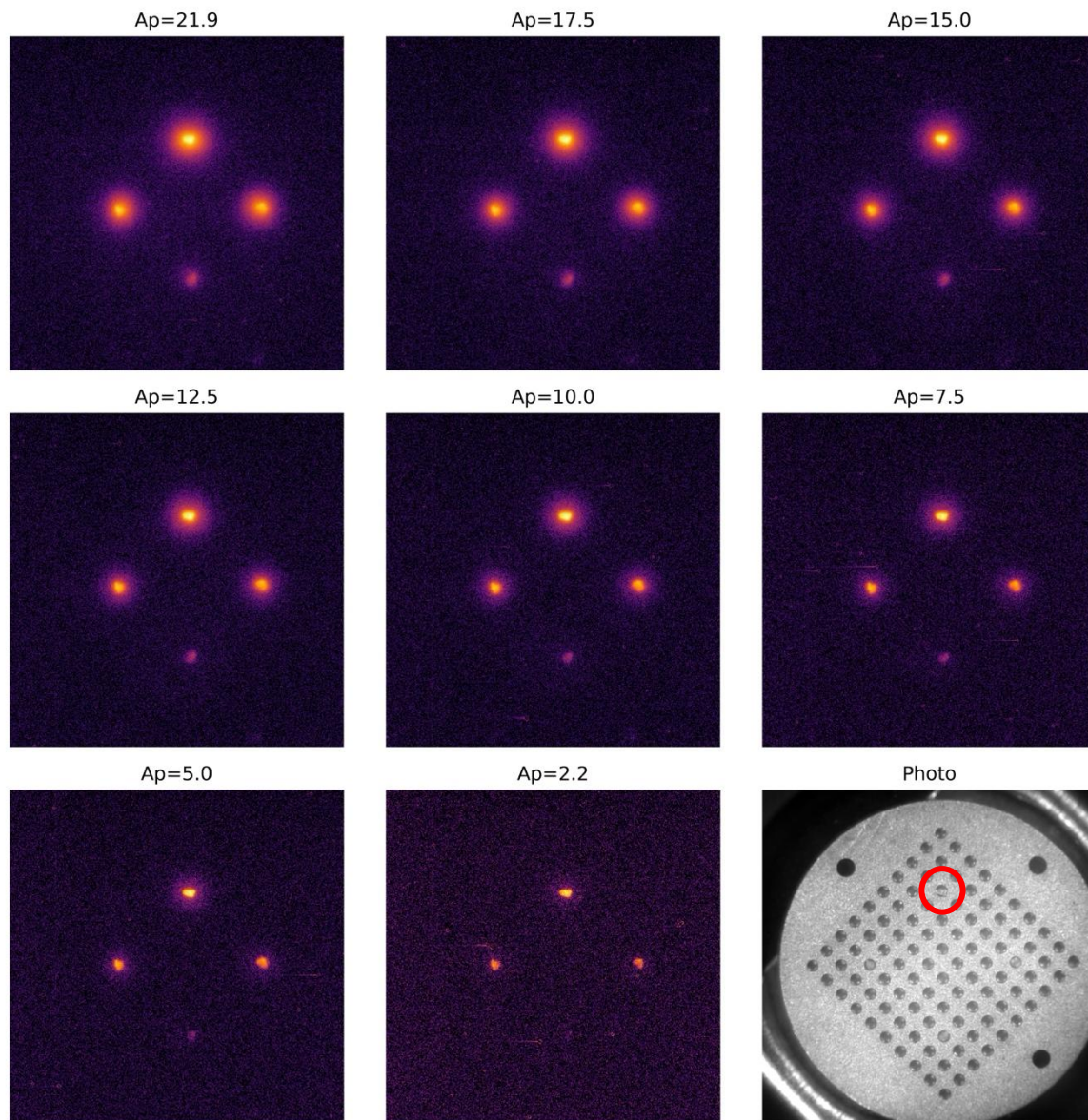


**Fig. 1.** Enhanced false colour images of the logarithm of the acquired luminescence for different apertures and the photo of the disc where four single grains can be seen. The TL has been integrated over the whole glow curve up to 220°C. The diameter of the aperture in mm is given above each image. The images get better defined with decreasing aperture; however, the intensity also decreases. The intensity scale is different for each image – see Fig. 2b – and hence no scale is shown. The red circle in the bottom right image emphasises grain no. 23.

important details. Firstly, it can be seen that the crosstalk increases dramatically as the aperture increases. For the largest aperture, the crosstalk reaches over 2.5% for position 24. This is a significant number given the previously published distributions of grain brightness (e.g. Duller, 2008). Secondly, we notice that the crosstalk is not symmetrical and probably depends on the shape of the grain and possibly on the area of the grain emitting the signal. The asymmetry can also be seen in the transect shown in Figs. 3a and 3b.

### 3.3 Excluding data impacted by crosstalk

Fig. 5 demonstrates that crosstalk between grains in adjacent positions on a single grain disc can reach 2.5%, and Fig. 4 shows that analysing ROI data from these adjacent positions could lead to incorrectly identifying a signal even where no sample exists. Two approaches are suggested here to avoid misidentification and reject signals arising from crosstalk.

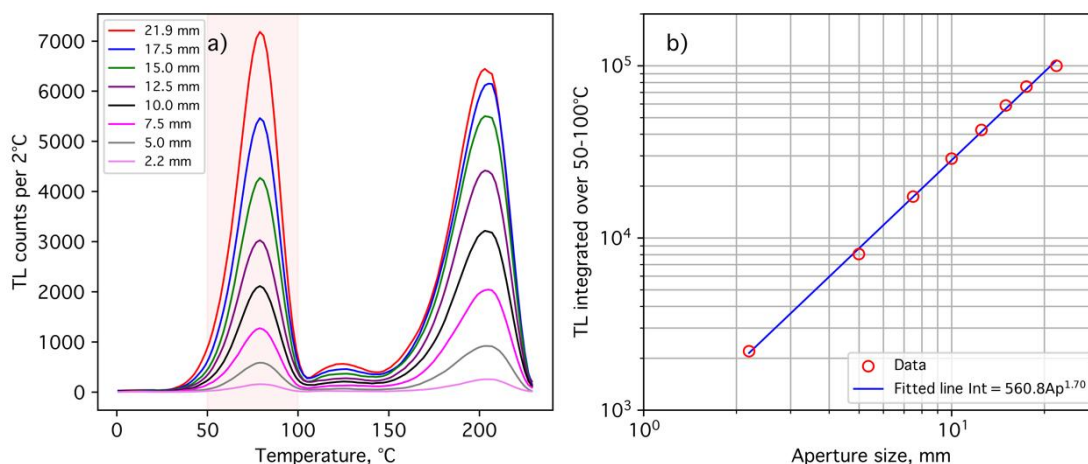


**Fig. 2.** a) Thermoluminescence glow curves for the grain in position 23 measured using apertures given in the legend. The signal plotted is obtained using a circular region of interest 300  $\mu\text{m}$  in diameter. b) The change in signal intensity from grain 23 due to changing aperture. The data is summed from 50 to 100°C (as shown by the shading in (a)). The data in (b) is fitted by a power function. Here, the exponent is equal to 1.70.

### 3.3.1 Peak identification

The first approach would be to look at the spatially-resolved luminescence data prior to segmentation using an ROI. A peak in the luminescence signal would be expected where a hole in the sample disc contains a grain emitting luminescence, and the intensity of this signal will decrease with distance away from the hole. The images shown in Fig. 1 illustrate this pattern clearly.

The same pattern can also be seen in the transect in Fig. 3b, where two peaks are seen, corresponding to the two holes in which grains were placed. One would be confident that any of the other grain holes (i.e. positions 21, 22, 24–27 and 29, 30) do not have a discernible signal because no peak in the luminescence signal is seen over those holes, and so when looking at Fig. 4 and 3b together, one would reject the data for positions 22 and 24.

This type of analysis would require looking at transects in both orientations. Taking the data from Fig. 2 and calculating a transect along holes 11 to 20 (all of which do not contain any quartz grains) would produce two peaks at holes 13 and 18 because of crosstalk from grains in hole positions 23 and 28. However, a transect perpendicular to this, for instance, from hole 3 to 93 would show a peak for hole 23 but not a peak for hole 13, thus making it clear that hole 13 does not contain a grain that generates a luminescence signal. Thus, this algorithm for verifying signals requires that a peak be observed when looking at profiles in both orientations.

The test dataset shown in Figs. 2 and 3 only has four grains across the whole disc. Normally, all 100 holes would contain grains, and so there is potential for situations where a hole may contain a grain which is emitting luminescence, and a peak would be seen in a transect such as Fig. 3b, but if there was a bright grain in an adjacent position then crosstalk from that bright grain would underlie the signal (e.g. Figs. 8a and 8c). In this situation, anal-

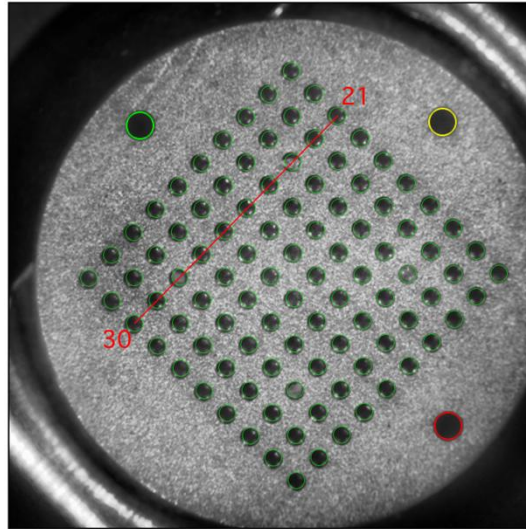
ysis of the transects would correctly identify the presence of a grain that is yielding a discernible signal, but the light summed within any ROI will also contain contributions from the adjacent bright grains.

To assess the magnitude of the crosstalk, one could envisage fitting the peaks in transects such as that shown in Fig. 8 (section 3.4), and thus calculating the contribution from adjacent signals. It would then be feasible to introduce some criterion for accepting or rejecting data from a hole (e.g. if the contribution from adjacent grains was less than 5%). The peaks seen in the TL transects (Fig. 3b) can be fitted with the sum of two Gaussian curves, both Gaussians having the same centre but with different width parameters. However, where peaks overlap (e.g., Fig. 8, section 3.4), the fitting is more complex, leading to large uncertainties. Thus, this approach has not been pursued further at this stage.

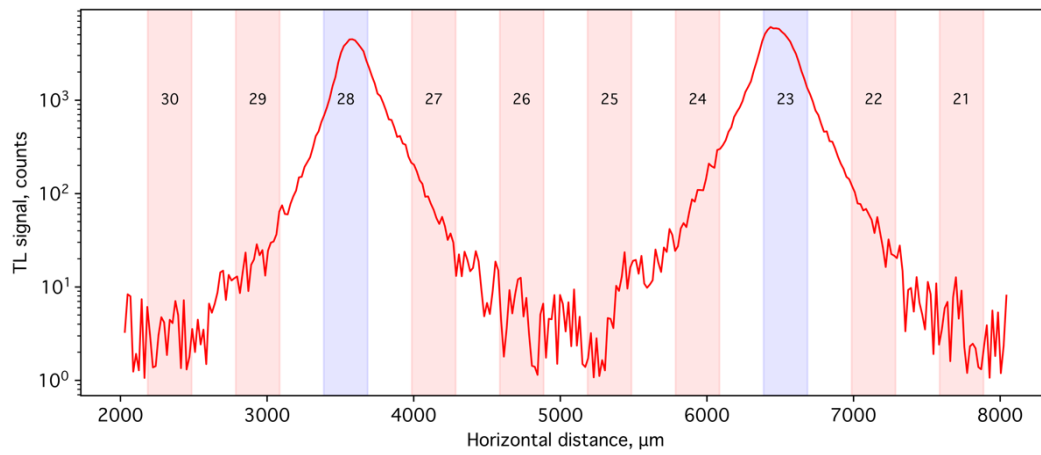
### 3.3.2 Adjacent position signal intensity

A simpler approach is to use the assessment of crosstalk derived from an experiment, as shown in Fig. 5, to estimate a maximum contribution from adjacent grain positions. In this case, a crosstalk of 2.5% is seen when using the largest aperture, so taking a conservative view, one could implement a rejection criterion whereby any grain that yields a signal that is *ca.* 10% or less than the sum of its neighbouring positions is rejected because it is likely to be impacted by crosstalk. The crosstalk, and hence this threshold, could be reduced by decreasing the aperture (Fig. 5), but this comes at the cost of reducing signal intensity (Fig. 1b). Additionally, as shown by Kook *et al.* (2015), the impact of adjacent grains can be reduced by making the ROI smaller, but this again comes at the cost of reducing the signal intensity and also introduces potential problems with signal reproducibility if only part of the grain hole is included in the ROI.

a)



b)



c)

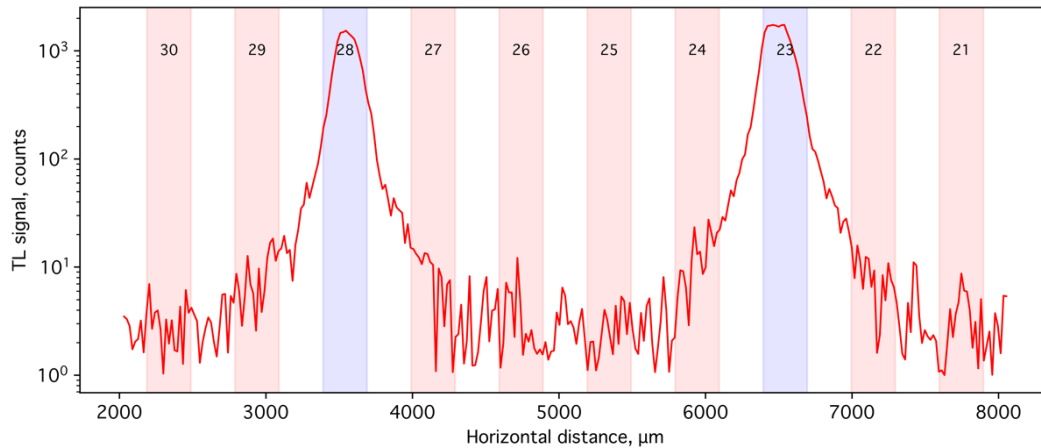


**Fig. 3.** A transect (b) through grains 30–21 of a width of 100  $\mu\text{m}$ , integrated over 50–100°C for the aperture of 21.9 mm. The shaded areas show hole positions indicated by the numbers in them, and a) shows the photo of the disc with the indicated line along which the transect was drawn, c) as b with an aperture of 10 mm.

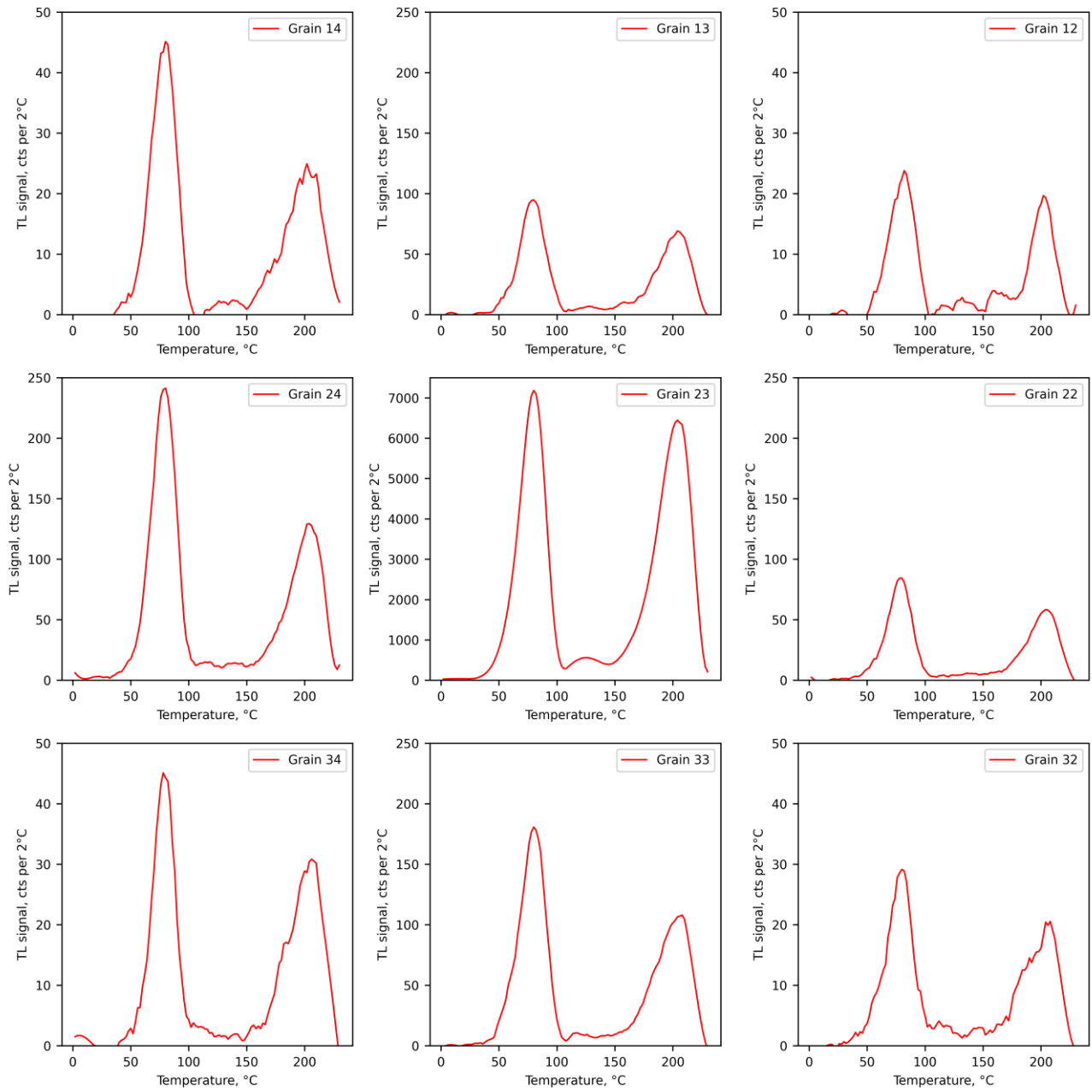


**Fig. 4.** Glow curves recorded around the brightest grain, no. 23 that was the brightest of the four grains. The ROI is a circular area of diameter 300  $\mu\text{m}$ , i.e. covering the area of the grain holding hole.

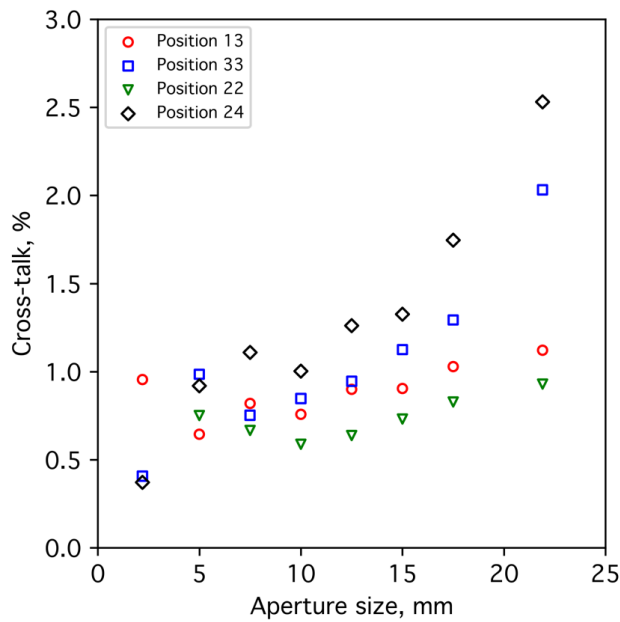


Fig. 5. Crosstalk for positions adjacent to grain no. 23 as a function of the aperture size. The ROI is a circular area of 300  $\mu\text{m}$  in diameter.

### 3.4 Changing the configuration of the single-grain disc

Another approach to reducing crosstalk, which does not decrease the sensitivity of the instrument, is to increase the spacing between holes on the single-grain disc. A compromise had to be struck between increasing the spacing between grains while still retaining enough grains on a single disc to maintain throughput. Taking into account the results of Fig. 3b, discs consisting of an array of 7 by 7 holes have been produced, with the hole diameter kept at 300  $\mu\text{m}$ , but spacing increased from 600  $\mu\text{m}$  between hole centres to 850  $\mu\text{m}$  between hole centres. Initially, we considered 5 by 5 hole discs, however, this would have reduced the number of grains measured by a quarter in relation to the original 10 by 10 discs and hence the decision to try a 7 by 7 arrangement.

The experiment described above (and shown in Figs. 1 to 3) was then repeated using a 7 by 7 single-grain disc. As it was noticed that in general the signals were dimmer, instead of the Hoya U-340 filter, the Shott BG39 filter was employed with maximum transmittance at 500 nm and FWHM of 210 nm. The lower light level is probably due to the fact that the reflectivity of stainless steel in UV is significantly lower than that of aluminium, from which the 10 by 10 discs are made. The application of the BG39 filter was to enable a broader wavelength range to be transmitted. The difference between the refractive indexes for quartz which make up the optical system lenses is about 0.015 between 340 and 500 nm which is not thought to introduce chromatic aberration that would explain the differences in crosstalk, especially since, as mentioned in section 2.1, the system adjusts for the changed focal length depending on the detection wavelength.

At first, four grains of the investigated sample were placed at positions 3, 7, 31 and 35 of the disc (Fig. 6a). We administered a dose of 280 Gy and heated the disc to 220°C. We then plotted a transect of the luminescence summed in the temperature range 50–100°C, across positions 29 to 35 (red line in Fig. 6a) of a width of 100  $\mu\text{m}$ . The transect is shown in Fig. 6b. Fig. 6b reveals that the distance between the grain holding holes ensures that the signal from adjacent holes does not interfere. This is further confirmed by the data shown in Fig. 7, where it can be seen that at the positions adjacent to grain 31, no measurable TL is detected. The crosstalk calculated as in section 3.2 is effectively zero.

To compare the performance of the two types of discs, transects of the emitted TL were drawn for positions 1–10 and 1–7 of the respective discs when they were loaded with grains in all of the holes. This was done for two aperture sizes, 21.9 mm (Figs. 8a and 8c) and 17.5 mm (Figs. 8b and 8d). We observe that the separation in the 7 by 7 disc is much better, and that decreasing the aperture to 17.5 mm gives even greater separation.

We conclude that the new discs lead to measurements with greatly reduced crosstalk. In the next section, we present an example of an analysis that can be carried out using the new discs.

## 4. Example of application: the 110°C TL peak in single grains of quartz

Here, for the first time, we are showing the determination of the lifetime of the “110°C” thermoluminescence (TL) peak in quartz for single grains using both the varying heating rate method and a direct measurement through varying delay times between irradiation and the readout.

### 4.1 Determination of trap parameters of the 110°C peak using variable heating rates

For the determination of the 110°C TL peak kinetic parameters, the Hoogenstraaten method (Hoogenstraaten, 1958) was used. The method utilises the changes in TL peak position with varying heating rates.

Three stainless steel discs with grids of 7 by 7 grains on each were each loaded with single grains of quartz from sample Aber105/KB15. These were irradiated with a dose of 93 Gy and then heated to 450°C at different heating rates, varying from 5°C s<sup>-1</sup> to 0.05°C s<sup>-1</sup>. An example of the TL glow curves recorded for one grain is displayed in Fig. 9a. Fig. 9b shows the peak positions of the “110°C” TL peak as a function of the heating rate. For each disc, the peak positions were calculated as averages of the peak positions for individual grains.

Fig. 9c shows the relationship between  $\ln(\beta/T^2)$  and  $-1/k_B T$  for one of the grains that was used to calculate the kinetic parameters of the electron trap responsible for the “110°C” TL peak (Hoogenstraaten, 1958; Wintle, 1975);  $k_B$  is the Boltzmann constant and  $T$  is the absolute temperature in K,  $\beta$  is the heating rate in Ks<sup>-1</sup>. The slope of

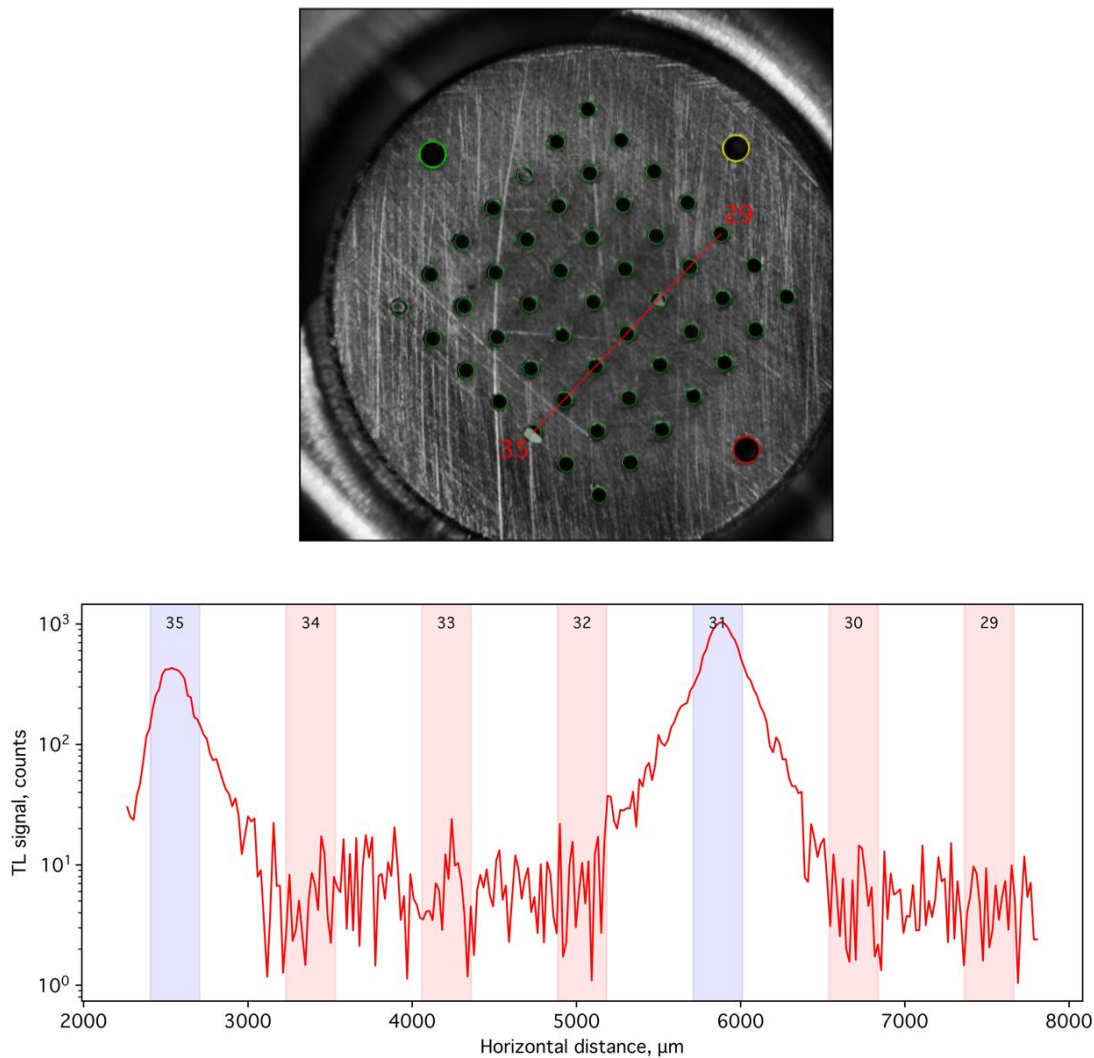


**Fig. 6.** As Figure 3 but for the 7x7 disc. Grains are in positions 1, 7, 31 and 35. Here, the transect extends from position 29 to 35, and the transect's width was ca. 100  $\mu\text{m}$  (5 pixels). The filter BG39 was used.

the fitted straight line is the depth of the trap ( $E$ ), and the frequency factor  $s$  is calculated from the intercept  $b$ , which is equal to

$$b = \ln\left(\frac{sk_B}{E-W}\right) \quad (4.1)$$

where  $E$  is the trap depth and  $W$  is the activation energy of thermal quenching. We assumed that the thermal quenching factor  $W$  is equal to zero as suggested, e.g. by Wintle (1975), who stated that the onset of thermal quenching of the UV emission centre occurs above ca. 100°C. Similarly, data presented by Friedrich *et al.* (2018) suggest that the quenching of the UV centre should be negligible below 100°C. However, it can be seen in Fig. 9a that the intensity of the peak increases with decreasing heating rate. In the current work, we could not determine whether thermal quenching is non-zero. This may be explored in future work.

At the higher heating rates (5 and 2°C s<sup>-1</sup>) the peak positions seen in different discs diverge (Fig. 9b), and for the experimental points seen in Fig. 9c deviate systematically from a fitted straight line. We therefore decided to reject these two heating rates, concluding that these were impacted by thermal lag. The resulting points and the fitted line are shown in Fig. 9d, where the experimental points lie on the fitted straight line. The obtained trap depth is higher than that which would have been calculated if the data for the 5 and 2°C s<sup>-1</sup> measurements had been included.

This analysis was repeated for all grains on the three discs. Fig. 10 summarises the results in the form of histograms of the peak temperatures (row 1), trap depths (row 2), logarithms of the frequency factors (row 3) and calculated lifetimes of the peak at 21°C. A temperature of 21°C was chosen rather than the usual 20°C, because this was the temperature measured inside the Risø reader during the

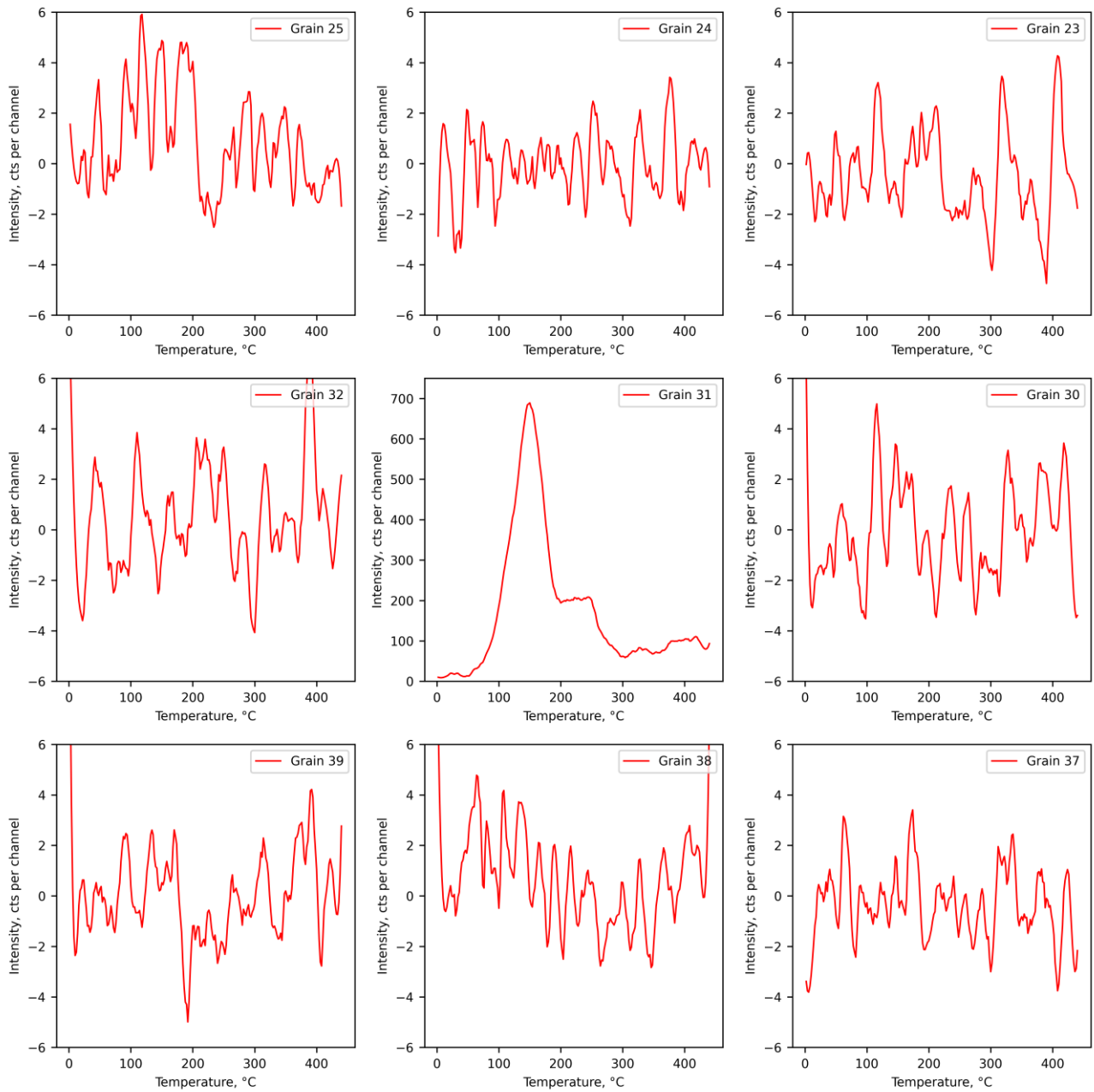


**Fig. 7.** Grain 31 and surrounding positions for ROI of diameter of 300  $\mu\text{m}$ , the aperture was 21.9. The filter BG 39 was used.

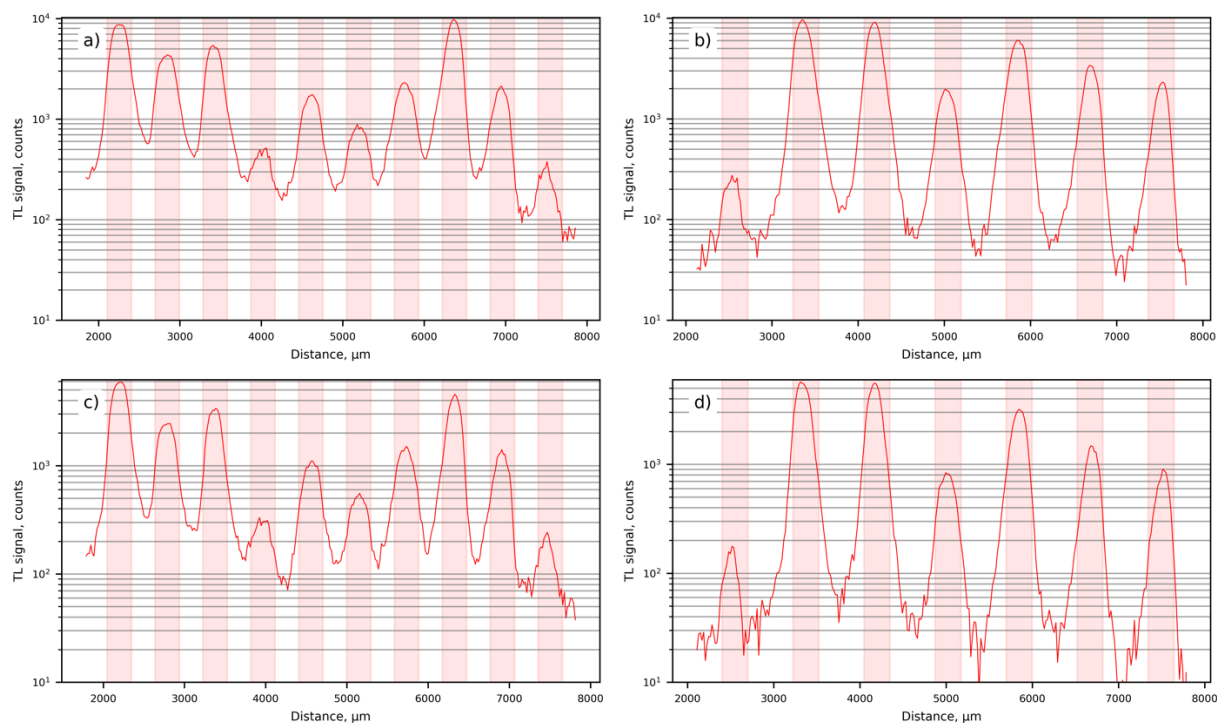


**Fig. 8.** Transects of the TL signal along one row of a 10 by 10 disc - a) and c); and 7 by 7 disc - b) and d). The top two plots (a and b) are taken with an aperture of 21.9 mm, and the lower ones (c and d) with an aperture of 17.5 mm. The shaded stripes indicate hole positions.

experiment described in the next section, and thus it allows direct comparison between the two sets of data.

From the peak positions (Fig. 10, top row), we can conclude that Disc 1 has the best thermal contact with the heating plate, as indicated by the “110°C” peak occurring at the lowest temperature among the three discs. Although the average peak position varies by only 1°C, this subtle difference supports the conclusion. Using data only from Disc 1, the average calculated lifetime of the “110°C” peak is 3517(33) s, where the quoted uncertainty is the standard error of the mean. Only data for grains where the maximum one-channel intensity of the lowest heating rate glow curve exceeded 150 counts were taken into account. The obtained trap depths are similar to those measured by others, e.g. Spooner and Questiaux (2000), and the frequency factors are of the expected order of magnitude.

This TL peak in quartz lends itself to a direct determination of the lifetime, and a comparison with the calculated value is explored in the next section.

#### 4.2 Direct determination of the lifetime of the 110°C peak

Since the lifetime of the 110°C peak is relatively short, it is practicable to make direct measurements of the lifetime by irradiating the sample and then storing it for different periods of time at a known temperature before measuring the intensity of the TL signal remaining. The same irradiation dose (93 Gy) was used for this experiment as for the Hoogenstraaten method. After irradiation, samples were

kept for periods of 0, 100, 200, 500, 1000, 2000, 5000 and 10000 s. Measurements for 0 and 1000 s were repeated at the end of the measurement cycle to check for any sensitivity changes, but these were found to be negligible. After the delay, the samples were heated at 5°C s<sup>-1</sup>, while the TL emission was measured with the EMCCD set with an aperture of 17.5 mm. The air conditioning in the laboratory is set to 20°C, while the temperature at which the samples were stored was about 21°C, as determined by a measurement of the temperature of the internal elements of the luminescence reader. It needs to be stressed that the actual storage temperature may be slightly different; however, a more accurate measurement was not attempted in the current experiments.

As expected, the intensity of the TL peak decreases with storage time, and the peak position remains consistent (Fig. 11a), as would be expected for a peak exhibiting first-order kinetics. When the TL intensity is plotted as a function of the time between irradiation and measurement (Fig. 11b), an exponential decay is observed, from which the lifetime of the signal can be determined. This analysis was repeated for all 49 hole positions on the disc, and 44 gave sufficient signal to allow a lifetime to be calculated. The mean lifetime was  $\tau_1=3700(44)$  s (Fig. 11c), where the uncertainty is the standard error of the mean.

This lifetime derived from the storage experiment and the lifetime of  $\tau_2=3517(33)$  s calculated from the kinetic parameters, do not overlap at two sigma

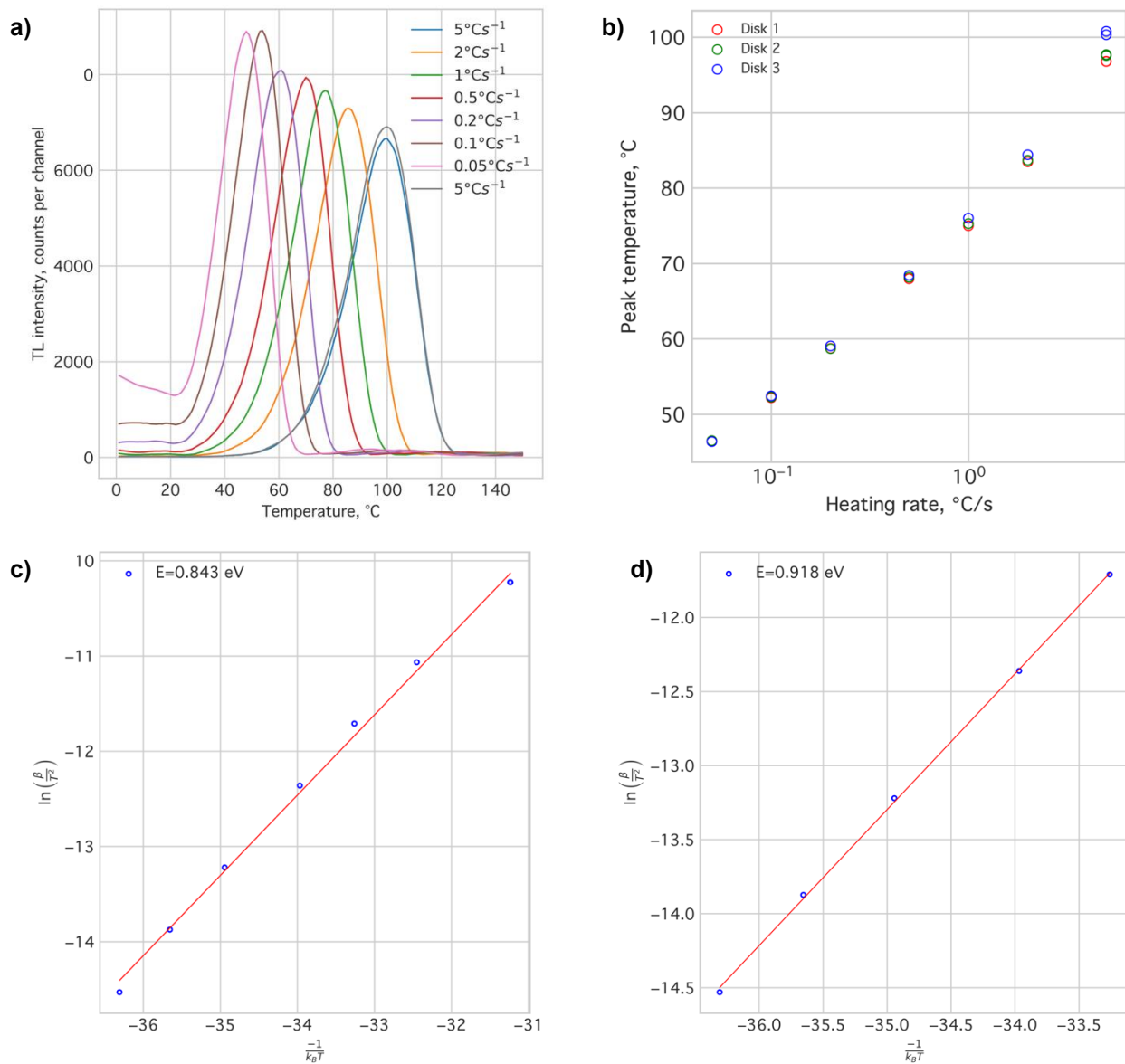


**Fig. 9.** a) TL glow curve recorded for a range of heating rates for one of the quartz grains, b) the average position of the “110°C” in three discs as a function of the heating rate, c) the plot of  $\ln(\beta/T_m^2)$  versus  $\frac{1}{k_B T}$  used to obtain the kinetic parameters for all recorded heating rates, d) the same graph after leaving out the heating rates of 5 and 2°C/s.

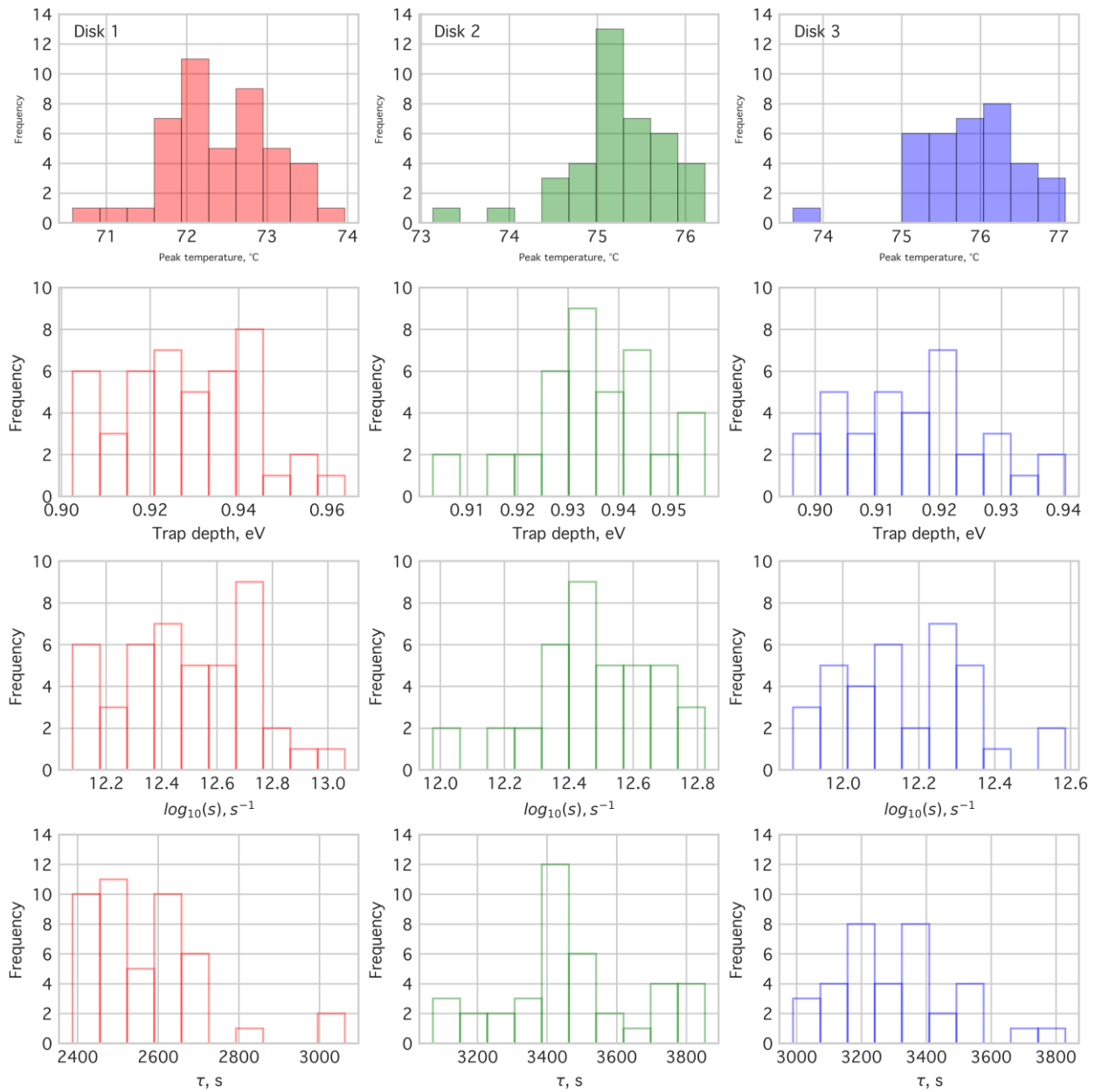


**Fig. 10.** The histograms of the 1st row: the 110°C position for three discs for the heating rate of  $1^\circ\text{C s}^{-1}$ , 2<sup>nd</sup> row: calculated trap depth, 3<sup>rd</sup> row:  $\log_{10}$  of the frequency factor and 4<sup>th</sup> row: the calculated lifetime of the peak at 21°C. The average lifetimes for discs 1, 2, and 3 are respectively 3517(33) s, 3474(32) s and 3305(32) s.

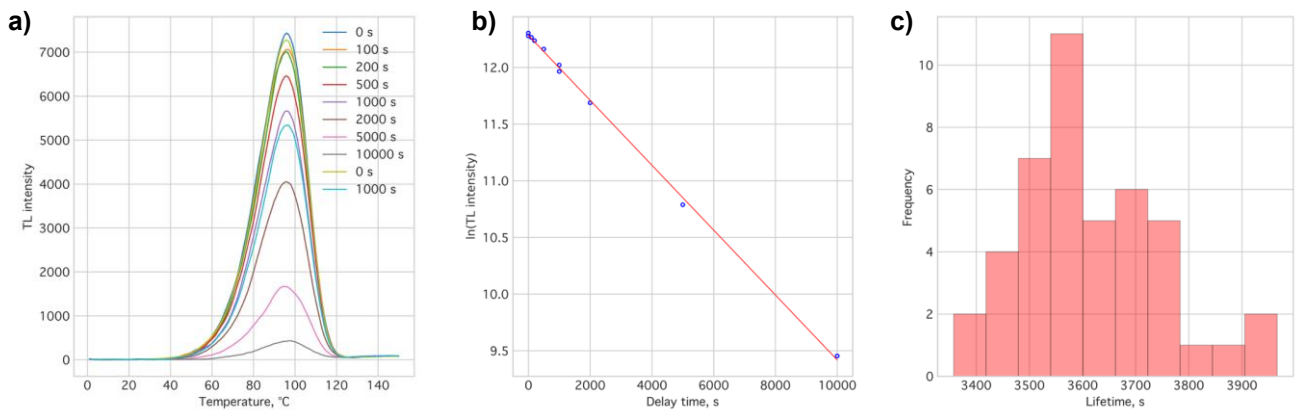


**Fig. 11.** The experiment to directly determine the lifetime of the 100°C peak. a) Glow curves from one of the grains for different delay times between irradiation and readout. The glow curves were recorded at 5°Cs<sup>-1</sup>, b) an example of ln(intensity) vs. delay time, c) the histogram of the lifetimes of the 110°C peak at a storage temperature of 21°C. The average lifetime is  $\tau_1=3700(44)$  s.

( $|\tau_1 - \tau_2|/\sqrt{\sigma_1^2 + \sigma_2^2} = 3.05$ ). However, the quoted error terms are only statistical, and they do not account for the fact that the storage temperature is not known with high accuracy, nor is the extent of thermal lag in the case of the measurements of the kinetic parameters. Therefore, we conclude that the agreement is satisfactory within the expected uncertainty, considering the experimental limitations.

## 5. Discussion

The analysis described in the previous sections aimed to characterise the pattern of crosstalk collected with the EMCCD system, where samples are spatially separated by mounting them on single grain discs containing an array of 10 by 10 grain holes. Unlike De Boer *et al.* (2024), we observe that with the current instrument and using the original discs supplied by the manufacturer, the crosstalk can be reduced by decreasing the size of the aperture used in the imaging system, but this reduction in crosstalk comes at the expense of the signal intensity (Fig. 1b), and the crosstalk into adjacent positions is never reduced to zero. It is not clear why De Boer *et al.* (2024) did not observe the same pattern; differences in experimental setup, optical alignment, or imaging parameters might account for the discrepancy. For our instrument, while the amount of crosstalk can be reduced to a low value (~1% is possible), if a sample consists of grains with very different intensities, then a bright grain could still impact the signal observed in ROIs surrounding the grain.

Crosstalk could lead to three types of error in analysis. The first is that positions where no grain is present could still yield a detectable signal (e.g. grains 21, 22, 24 and 25 in Fig. 3b) which would be thought to be a discrete grain, but the behaviour of the signals from these ‘phantom’ grains would be identical to that of the grain from which the light originates. In the example shown in Fig. 3, the

signal from grains 21, 22, 24 and 25 originates from only one grain (that in position 23), but where a larger number of grains emit a signal on a disc, then the signal observed may be a complex mixture of nearby grains. If chemical analysis of the grains in the disc were undertaken, for instance, using laser ablation inductively coupled plasma-mass spectrometry (Smedley *et al.*, 2012), then no grain would be found. The second error is similar to the first, except in this scenario, there is a grain present in a hole, but any emission is too weak to be observed, so once again, the signal may originate from crosstalk. In this instance, any attempt to, for example, correlate chemical characteristics with luminescence behaviour would be unlikely to succeed. The third possible error is where a grain is present, and it emits a detectable luminescence signal, but crosstalk from adjacent grains is also contained within the ROI. This scenario results in a mixture of signals, both from the grain and from adjacent grains. The relative intensity of the various grains will control the extent to which the observed luminescence characteristics originate from the grain being measured or its neighbours.

While it may not be possible to reduce crosstalk to zero when using the sample disc with 10 by 10 holes, the distribution of emitted luminescence does provide the possibility to discern whether the signal measured in an ROI originates from that sample hole or not. Scenario 1 described above can be seen in Fig. 3. A TL signal is observed in the ROI data for all five grain positions (positions 21–25, Fig. 3b), but analysis of the ROI data alone would not be able to decide whether these signals arose from 5 separate grains or not. However, the pattern of luminescence intensity in the transect along that row of grain positions demonstrates that there is a peak in emission associated with position 23, but no peak is seen for any of the other 4 positions. Analysis of transects across the luminescence images provides the potential for deciding whether the emission is occurring from any individual position by looking for a peak. If no peak is found, then any signal

from an ROI associated with that position is likely to arise from crosstalk and should not be included in any further analysis.

Reducing the number of grains on the sample disc to 7 by 7 increases the spacing between the grains and makes it possible to reduce the crosstalk to near zero (Figs. 7, 8b and 8d). Although this means that the number of grains on a disc is reduced by a factor of two compared with the original 10 by 10 disc, the dramatic reduction in crosstalk means that the integrity of the data is superior.

## 6. Conclusions

The EMCCD system used in this paper opens exciting new possibilities for the study of luminescence phenomena. Its integration into an automated system capable of making a range of luminescence measurements and irradiating a sample under computer control (Kook *et al.*, 2015) provides a powerful research tool. However, as with all instruments, it is important to understand the limitations. When using sample discs with an array of 10 by 10 holes spaced 600  $\mu\text{m}$  apart, and using the imaging system currently implemented, signal crosstalk is a problem. There are ways of screening data to avoid misidentification of “ghost” grains (i.e. seeing a signal where no grain is present), but where signals overlap from adjacent grains, it is complex to attempt to disentangle them. This study has looked at the TL signal from quartz to characterise this crosstalk, but since the crosstalk is the result of the imaging system, we would expect that the same crosstalk issues will impact any measurement of optically stimulated luminescence (OSL) or thermoluminescence (TL) signal, whether that be from quartz, feldspar or other material.

The most effective solution to reduce the impact of crosstalk is to increase the spacing between grains, and the 7 by 7 disc appears to be a good compromise between keeping sufficient grains on each disc to maintain

throughput as originally envisaged for single grains, but significantly reducing crosstalk, thus simplifying processing and analysis, and improving the integrity of the data obtained. The new discs should be manufactured from aluminium to enable as much light efficiency as possible.

Using the new disc design, we determined the trap parameters of the 110°C peak at the single-grain level. We applied the varying heating rate method to ascertain the lifetime of electrons trapped in the trap. We then compared the calculated lifetime with the lifetime determined directly in a storage experiment for the first time for single grains, achieving excellent agreement. This demonstrates the potential for future basic research in EMCCD measurements.

## Acknowledgements

The one-month stay of Grzegorz Adamiec at Aberystwyth University was supported under the Silesian University of Technology Rector’s professorial grant implemented as part of the Excellence Initiative – Research University program, grant number 14/020/SDU/10-07-01.

Capital funding for the EMCCD was from HEFCW to support the creation of the SPARCL (SPATIALLY Resolved geoChronoLogY) facility in the Department of Geography and Earth Sciences at Aberystwyth University.

## Declaration of generative AI and AI-assisted technologies in the writing process

During the preparation of this work, the author(s) used chatGPT 4o in order to correct the language. After using this tool/service, the author(s) reviewed and edited the content as needed and take(s) full responsibility for the content of the publication.

## References

- Adamiec G, 2000. Variations in luminescence properties of single quartz grains and their consequences for equivalent dose estimation. *Radiation Measurements* 32(5–6): 427–432, DOI [10.1016/s1350-4487\(00\)00043-3](https://doi.org/10.1016/s1350-4487(00)00043-3).
- Bailiff I and Mikhailik V, 2003. Spatially-resolved measurement of optically stimulated luminescence and time-resolved luminescence. *Radiation Measurements* 37(2): 151–159, DOI [10.1016/s1350-4487\(02\)00187-7](https://doi.org/10.1016/s1350-4487(02)00187-7).
- Bøtter-Jensen L, Andersen C, Duller G and Murray A, 2003. Developments in radiation, stimulation and observation facilities in luminescence measurements. *Radiation Measurements* 37(4–5): 535–541, DOI [10.1016/s1350-4487\(03\)00020-9](https://doi.org/10.1016/s1350-4487(03)00020-9).
- Bradski G, 2000. The OpenCV library. *Dr. Dobb’s Journal* 25(11): 120–125.
- Bulur E, Duller G, Solongo S, Bøtter-Jensen L and Murray A, 2002. LM-OSL from single grains of quartz: a preliminary study. *Radiation Measurements* 35(1): 79–85, DOI [10.1016/s1350-4487\(01\)00256-6](https://doi.org/10.1016/s1350-4487(01)00256-6).
- de Boer A, Kook M and Wallinga J, 2024. Testing the performance of an EMCCD camera in measuring single-grain feldspar (thermo)luminescence in comparison to a laser-based single-grain system. *Radiation Measurements* 175107168, DOI [10.1016/j.rad-meas.2024.107168](https://doi.org/10.1016/j.rad-meas.2024.107168).
- Duller GAT, 2008. Single-grain optical dating of Quaternary sediments: why aliquot size matters in luminescence dating. *Boreas* 37(4): 589–612, DOI [10.1111/j.1502-3885.2008.00051.x](https://doi.org/10.1111/j.1502-3885.2008.00051.x).
- Duller GAT, 2012. Cross-talk during single grain optically stimulated luminescence measurements of quartz and feldspar. *Radiation Measurements* 47(3): 219–224, DOI [10.1016/j.rad-meas.2011.12.006](https://doi.org/10.1016/j.rad-meas.2011.12.006).
- Duller GAT, Bøtter-Jensen L and Murray A, 2000. Optical dating of single sand-sized grains of quartz: sources of variability. *Radiation Measurements* 32(5–6): 453–457, DOI [10.1016/s1350-4487\(00\)00055-x](https://doi.org/10.1016/s1350-4487(00)00055-x).
- Duller GAT, Bøtter-Jensen L and Markey B, 1997. A luminescence imaging system based on a CCD camera. *Radiation Measurements* 27(2): 91–99, DOI [10.1016/s1350-4487\(96\)00120-5](https://doi.org/10.1016/s1350-4487(96)00120-5).
- Duller GAT, Bøtter-Jensen L, Murray A and Truscott A, 1999. Single grain laser luminescence (SGLL) measurements using a novel automated reader. *Nuclear Instruments and Methods in Physics Research Section B: Beam Interactions with Materials and Atoms* 155(4): 506–514, DOI [10.1016/s0168-583x\(99\)00488-7](https://doi.org/10.1016/s0168-583x(99)00488-7).

- Duller GAT, Tooth S, Barham L and Tsukamoto S, 2015. New investigations at Kalambo Falls, Zambia: Luminescence chronology, site formation, and archaeological significance. *Journal of Human Evolution* 85:111–125, DOI [10.1016/j.jhevol.2015.05.003](https://doi.org/10.1016/j.jhevol.2015.05.003).
- Durcan JA and Duller GAT, 2022. The variability of single grain quartz luminescence properties investigated using EMCCD imaging. *Radiation Measurements* 153:106748, DOI [10.1016/j.radmeas.2022.106748](https://doi.org/10.1016/j.radmeas.2022.106748).
- Durcan JA and Duller GAT, 2024. Further investigation of spatially resolved single grain quartz OSL and TL signals. *Radiation Measurements* 177:107260, DOI [10.1016/j.radmeas.2024.107260](https://doi.org/10.1016/j.radmeas.2024.107260).
- Friedrich J, Kreutzer S and Schmidt C, 2018. Radiofluorescence as a detection tool for quartz luminescence quenching processes. *Radiation Measurements* 120: 33–40, DOI [10.1016/j.radmeas.2018.03.008](https://doi.org/10.1016/j.radmeas.2018.03.008).
- Greilich S, Gribenski N, Mittelstraß D, Dornich K, Huot S and Preusser F, 2015. Single-grain dose-distribution measurements by optically stimulated luminescence using an integrated EMCCD-based system. *Quaternary Geochronology* 29:70–79, DOI [10.1016/j.quageo.2015.06.009](https://doi.org/10.1016/j.quageo.2015.06.009).
- Gribenski N, Preusser F, Greilich S, Huot S and Mittelstraß D, 2015. Investigation of cross talk in single grain luminescence measurements using an EMCCD camera. *Radiation Measurements* 81: 163–170, DOI [10.1016/j.radmeas.2015.01.017](https://doi.org/10.1016/j.radmeas.2015.01.017).
- Hoogenstraaten W, 1958. Electron traps in zinc sulphide phosphors. *Philips Research Reports* 13: 515–562.
- Kook M, Lapp T, Murray A, Thomsen K and Jain M, 2015. A luminescence imaging system for the routine measurement of single-grain OSL dose distributions. *Radiation Measurements* 81: 171–177, DOI [10.1016/j.radmeas.2015.02.010](https://doi.org/10.1016/j.radmeas.2015.02.010).
- Mittelstraß D and Kreutzer S, 2021. Spatially resolved infrared radiofluorescence: single-grain K-feldspar dating using CCD imaging. *Geochronology* 3(1): 299–319, DOI [10.5194/gchron-3-299-2021](https://doi.org/10.5194/gchron-3-299-2021).
- Roberts RG, Jacobs Z, Li B, Jankowski NR, Cunningham AC and Rosenfeld AB, 2015. Optical dating in archaeology: thirty years in retrospect and grand challenges for the future. *Journal of Archaeological Science* 56:41–60, DOI [10.1016/j.jas.2015.02.028](https://doi.org/10.1016/j.jas.2015.02.028).
- Savitzky A and Golay MJE, 1964. Smoothing and Differentiation of Data by Simplified Least Squares Procedures. *Analytical Chemistry* 36(8): 1627–1639, DOI [10.1021/ac60214a047](https://doi.org/10.1021/ac60214a047).
- Singarayer J and Bailey R, 2003. Further investigations of the quartz optically stimulated luminescence components using linear modulation. *Radiation Measurements* 37(4–5): 451–458, DOI [10.1016/s1350-4487\(03\)00062-3](https://doi.org/10.1016/s1350-4487(03)00062-3).
- Smedley RK, Duller GAT, Pearce NJG and Roberts HM, 2012. Determining the K-content of single-grains of feldspar for luminescence dating. *Radiation Measurements* 47(9): 790–796, DOI [10.1016/j.radmeas.2012.01.014](https://doi.org/10.1016/j.radmeas.2012.01.014).
- Smith BW, Wheeler G, Rhodes EJ and Spooner NA, 1991. Luminescence dating of zircon using an imaging photon detector. *International Journal of Radiation Applications and Instrumentation. Part D. Nuclear Tracks and Radiation Measurements* 18(1–2): 273–278, DOI [10.1016/1359-0189\(91\)90122-x](https://doi.org/10.1016/1359-0189(91)90122-x).
- Spooner NA and Questiaux D, 2000. Kinetics of red, blue and UV thermoluminescence and optically-stimulated luminescence from quartz. *Radiation Measurements* 32(5–6): 659–666, DOI [10.1016/s1350-4487\(00\)00067-6](https://doi.org/10.1016/s1350-4487(00)00067-6).
- Templer R and Walton A, 1985. Zoning in zircons. *Nuclear Tracks and Radiation Measurements (1982)* 10(4–6): 683–692, DOI [10.1016/0735-245x\(85\)90076-6](https://doi.org/10.1016/0735-245x(85)90076-6).
- Virtanen P, Gommers R, Oliphant TE, Haberland M, Reddy T, Cournapeau D, Burovski E, Peterson P, Weckesser W, Bright J, van der Walt S J, Brett M, Wilson J, Millman K J, Mayorov N, Nelson ARJ, Jones E, Kern R, Larson E, ... Vázquez-Baeza Y, 2020. SciPy 1.0: fundamental algorithms for scientific computing in Python. *Nature Methods* 17(3): 261–272, DOI [10.1038/s41592-019-0686-2](https://doi.org/10.1038/s41592-019-0686-2).
- van der Walt S, Schönberger JL, Nunez-Iglesias J, Boulogne F, Warner JD, Yager N, Gouillart E and Yu T, 2014. scikit-image: Image processing in Python. *PeerJ PrePrints* 2, DOI [10.7287/peerj.preprints.336v1](https://doi.org/10.7287/peerj.preprints.336v1).
- Wallinga J, 2002. On the detection of OSL age overestimation using single-aliquot techniques. *Geochronometria* 21: 17–26. [https://www.geochronometria.pl/pdf/geo\\_21/Geo21\\_02.pdf](https://www.geochronometria.pl/pdf/geo_21/Geo21_02.pdf)
- Wintle AG, 1975. Thermal Quenching of Thermoluminescence in Quartz. *Geophysical Journal International* 41(1): 107–113, DOI [10.1111/j.1365-246x.1975.tb05487.x](https://doi.org/10.1111/j.1365-246x.1975.tb05487.x).
- Yukihara EG, McKeever SW and Akselrod MS, 2014. State of art: Optically stimulated luminescence dosimetry – Frontiers of future research. *Radiation Measurements* 71: 15–24, DOI [10.1016/j.radmeas.2014.03.023](https://doi.org/10.1016/j.radmeas.2014.03.023).